Original Article

Institution of MECHANICAL ENGINEERS
Journal of ENGINEERING TRIBOLOGY

Proc IMechE Part J:
J Engineering Tribology
2020, Vol. 234(1) 126–133

DOI: 10.1177/1350650119855594
journals.sagepub.com/home/pij
SAGE

An elastoplastic finite element study of cylindrical plane-strain contact for steel/steel and Inconel 617/Incoloy 800H undergoing unidirectional sliding

Huaidong Yang and Itzhak Green

Abstract

The current work employs a two-dimensional plane strain finite element analysis to investigate the unidirectional sliding contact between a deformable half-cylinder and a deformable flat block. The unidirectional sliding is governed by a displacement-controlled action where the materials of the two contacting bodies are first set to identical steels at 20 °C and then to Inconel 617 and Incoloy 800H at 800 °C. First, a normal interference (indentation) is applied, which is followed by unidirectional sliding. The von Mises stress distribution, plastic strain distribution, junction growth, normal force, tangential force, effective coefficient of friction, and scars on the surface of the block are obtained during the sliding motion. The leading edge of the contacting area and the bulk material under the leading edge experience large von Mises stresses. The large plastic strain is found on the surface of the block, and forms a "pocket" shape under the surface. The junction growth is also investigated, showing the direction of the growth is in the same direction of the tangential force that the weaker material experiences. The forces and the effective coefficient of friction are found to stabilize after a certain sliding distance, and the effective coefficient of friction converges to the coefficient of friction used in the model. Pileup is found on the surface of the block after a sufficient unidirectional sliding distance.

Keywords

Cylindrical contact, elastoplastic wear, finite element method/analysis, plane strain, unidirectional sliding

Date received: 17 January 2019; accepted: 14 May 2019

Introduction

Unidirectional sliding contact is prevalent in rolling bearings, wheel–rail controls, and head–disk interactions. Additionally, understanding the mechanics of sliding contacts provides a foundation for fretting damage analysis. Therefore, it is meaningful to study sliding contact as a tribological building block phenomenon.

Various theoretical works have been done to analyze sliding contact under different conditions. The solutions of contact pressure, tangential force, and deformation for elastic surface were provided by Johnson.[1] Following that, Chang and Zhang[2] established a mathematical model for the elastic-plastic sphere-on-flat contacts. Junction growth, i.e. the increase of the contact area, was reported.

Experimental works have also been done to analyze the sliding contact. The stress field in a sliding frictional contact was studied by Scheibert by using a microelectromechanical systems–based sensing device.[3] Courtney-Pratt and Eisner[4] studied the metallic sliding contacts between a sphere and a flat surface, showing junction growth. Junction growth was also found by Tabor[5] and Parker and Hatch.[6] Pileup was recorded by Bellemare,[7] who also investigated the effect of the strain hardening.

Numerical methods using the finite element model are applied to the study of stick and sliding contact,[8–10] which focus on the initial stage of yielding under full stick, partial slip, and full slip conditions, including the effect of coating. Holmberg[11] studied the stress field, plastic strain, and the pileup for spherical sliding contacts. However, the studies above are all modeling the contacts in three dimensions. The only two-dimensional finite element analysis works found for sliding contacts are of Vijaywargiya and Green[12] and Tian and Saka.[13] Vijaywargiya and Green[12]

School of Mechanical Engineering, Georgia Institute of Technology, Atlanta, GA, USA

Corresponding author:
Itzhak Green, School of Mechanical Engineering, Georgia Institute of Technology, Atlanta, GA 30332-0405, USA.
Email: itzhak.green@me.gatech.edu

modeled the two-dimensional sliding contact with two interfering cylinders in the regime of elastic-plastic contacts. Deformations, reaction forces, stresses, and energy losses as a function of the interference and sliding distance were discussed. But, since it was between identical cylinders, the contacts between a tip and a flat surface could not be studied, especially for the scars on the flat surface. Hong and Nannaji[13] modeled their contact between a rigid cylinder and an elastic half-space. However, they used the load-controlled analysis, and their results were not generalized or normalized.

In this work, a unidirectional sliding displacement-controlled contact model between a deformable half-cylinder and a deformable block is generated. An interference is first applied to the top of the cylinder, which introduces an elastic-plastic contact. The unidirectional sliding motion is then started. The materials of the two bodies are first set to be identical steels to study contacts between similar materials. Then, dissimilar materials, Inconel 617 and Incoloy 800H at 800 °C, are studied, both of which are promising structural materials for high temperature and very high temperature gas-cooled reactors (HTGRs/VHTRs). The von Mises stress, plastic strain, forces, effective coefficient of friction (COF), and the scars on the surface of the block are reported during the sliding motions. The objective is to form an in-depth understanding of the mechanisms of sliding wear, the propensity for crack initiation, and propagation. Additionally, it forms the foundation for a fretting wear analysis done by Yang and Green[14] between identical steels and Incoloy 800H/Inconel 617.[15]

The model

The sliding contact in this work is between a half-cylinder of radius $R = 0.5\,\text{m}$ and a $4\text{R} \times \text{R}$ block as shown in Figure 1(a). The coordinate system is shown with the origin point located at the initial contact point. The two material schemes are listed in Table 1. In scheme 1, the two bodies are identical steels at room temperature (20 °C), while in scheme 2, the cylinder is Inconel 617 at 800 °C and the block is Incoloy 800H at 800 °C. The material properties are listed in Table 2.[16] The yield strength of Incoloy 800H is about one-third of that of Inconel 617 at 800 °C. The elastic-perfectly plastic behavior is used in the finite element analysis. Adhesion and wear are not included in this work.

The sliding model is shown in Figure 1(b). First, a vertical displacement, ω, is applied on the top of the half-cylinder and is kept constant all the time. That is referred to as the interference. Then a horizontal displacement, δ, is applied to simulate the sliding motion. The sliding motion is in the direction of positive X, which is implicitly referred to as "right". The analysis is quasi-static without dynamic effects.

In the regime of static elastic normal contact, the Hertzian theory gives the solution to the 2D plane strain cylindrical contact. Given a normal load per unit length, P/L, the maximum pressure, p_0 is located at the center of the contact[1]

$$p_0 = \frac{2P}{\pi b L} \tag{1}$$

The half-width of contact, b, is given by

$$b = \left(\frac{4PR}{\pi L E'}\right)^{\frac{1}{2}} \tag{2}$$

Table 1. Material schemes in the model.

Scheme	Cylinder	Block
1	Steel	Steel
2	Inconel 617 (800 °C)	Incoloy 800H (800 °C)

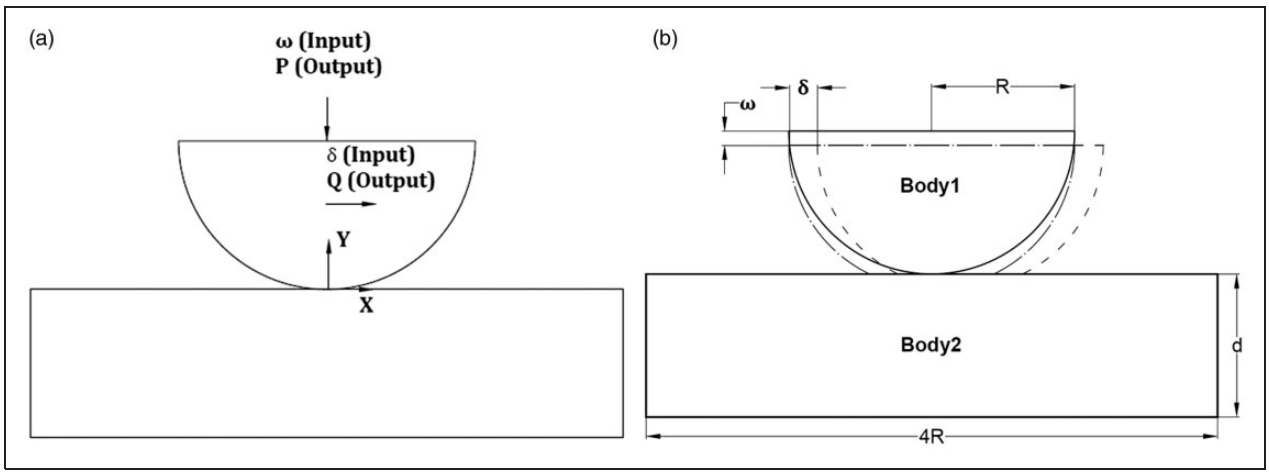

Figure 1. Schematic of a half-cylinder in contact with a flat block, along with the loading definitions: (a) displacement-controlled inputs and reaction outputs; (b) cylinder-block dimensions and displacement directions.

Table 2. Material properties of Inconel alloy 617 and Incoloy alloy 800H at 800 °C, and steels used in the model.

Materials	Elastic modulus, E (GPa)	Yielding strength, S_y (MPa)	Poisson's ratio, v	$C(\nu)$	$C{\cdot}S_y$ (MPa)
Inconel 617	157.0	290	0.3	1.795	521
Incoloy 800H	141.3	90	0.394	1.839	170
Steel	200.0	911	0.32	1.818	1657

Table 3. The critical values for different material schemes.

Scheme	Critical interference (μm)	Critical load per unit length (MN/m)	Critical half-contact width (mm)
1	$\omega_{c1} = 927$	$P_{c1}/L = 38.7$	$b_{c1} = 14.9$
2	$\omega_{c2} = 24.5$	$P_{c2}/L = 0.532$	$b_{c2} = 2.0$

where E' is the equivalent elastic modulus given by

$$\frac{1}{E'} = \frac{1-\nu_1^2}{E_1} + \frac{1-\nu_2^2}{E_2} \tag{3}$$

where E_1 and ν_1 represent the elastic modulus and Poisson's ratio of the cylinder, while E_2 and ν_2 represent the elastic modulus and Poisson's ratio of the block.

The interference of a half-cylinder in contact with a block, whose depth is d, is derived in another paper by Yang and Green[14]

$$\begin{aligned}\omega = {} & \frac{P}{L}\frac{(1-\nu_1{}^2)}{\pi E_1}\left\{\ln\left(\frac{4\pi E' R}{P/L}\right) - 1\right\} \\ & + \frac{P}{L}\frac{(1-\nu_2{}^2)}{\pi E_2}\left\{\ln\left(\frac{\pi d^2 E'}{RP/L}\right) - \frac{\nu_2}{(1-\nu_2)}\right\}\end{aligned} \tag{4}$$

According to Green,[17] for contact between dissimilar materials, the minimum of the products of C_1S_{y1} and C_2S_{y2} determines the maximum contact pressure, p_0, at the onset of material yielding. Hence, as $C(\nu) = 1.164 + 2.975\nu\text{-}2.906\nu^2$, for $\nu > 0.1938$, the product is

$$CS_y = \min\left\{C_1S_{y1}, C_2S_{y2}\right\} \tag{5}$$

The values C_1 and S_{y1} represent the properties of the cylinder, where C_2 and S_{y2} represent the properties of the block. Based on Table 2, for scheme 1, the two identical steels yield simultaneously, while in scheme 2, Incoloy 800H is the weaker material that yields first.

The critical half-contact width, b_c, and the critical load per unit length, P_c/L, at which the maximum von Mises stress reaches the yield strength, S_y, in the weaker material are derived by Green[17]

$$b_c = \frac{2RCS_y}{E'} \tag{6}$$

$$\frac{P_c}{L} = \frac{\pi R(CS_y)^2}{E'} \tag{7}$$

By subsisting equation (7) into equation (4), the critical interference is given as

$$\begin{aligned}\omega_c = {} & \frac{R(CS_y)^2(1-\nu_1^2)}{E'E_1}\left[2\ln\left(\frac{2E'}{CS_y}\right) - 1\right] \\ & + \frac{R(CS_y)^2(1-\nu_2^2)}{E'E_2}\left[2\ln\left(\frac{dE'}{RCS_y}\right) - \frac{\nu_2}{1-\nu_2}\right]\end{aligned} \tag{8}$$

For the material properties and the depth of the block ($d = R$) herein, the critical interference, the critical load per unit length, and the critical half-contact width for different material schemes are given in Table 3.

Subsequent results are normalized by their corresponding critical values. In this work, the values of the vertical interference are integer multiples of the critical one, namely $1*\omega_{c1}$, $2*\omega_{c1}$, $3*\omega_{c1}$, etc. in scheme 1 and $1*\omega_{c2}$, $2*\ \omega_{c2}$, $3*\omega_{c2}$, etc. in scheme2. The maximum horizontal displacement is $5*\omega_{c1}$ in scheme 1 and $5*\omega_{c2}$ in scheme 2. In this way, the results are readily nondimensionalized and they can be applied to both macroscopic and microscopic contacts. In this displacement-controlled simulation, the vertical interference and the horizontal displacement, ω and δ, are the inputs, while the normal and tangential forces at the contact, P and Q, are outputs.

Mesh converge

Elements PLANE183 is used to mesh the model in ANSYS 17.1 (shown in Figure 2). There are 58,103 elements for scheme 1 and 50,042 elements for scheme 2. The size of the refined mesh in the contact area is 8×10^{-4}R for scheme 1, and 8×10^{-5}R for scheme 2. One-hundred contact elements (CONTA172 and TARGE169) on each side of the contact are used to simulate the frictional contacts.

This work utilizes the same model as steel-on-steel contacts in Yang and Green[14] and Inconel

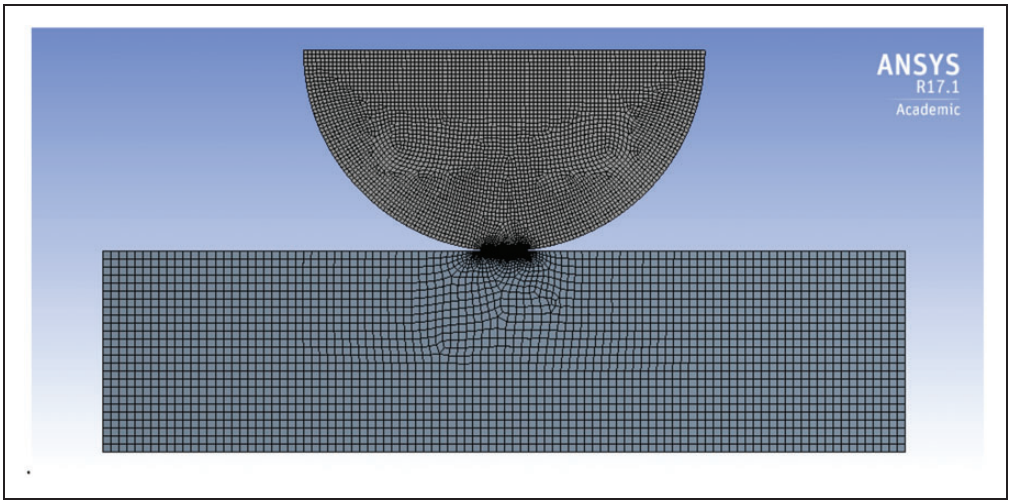

Figure 2. Finite element model in ANSYS 17.1.

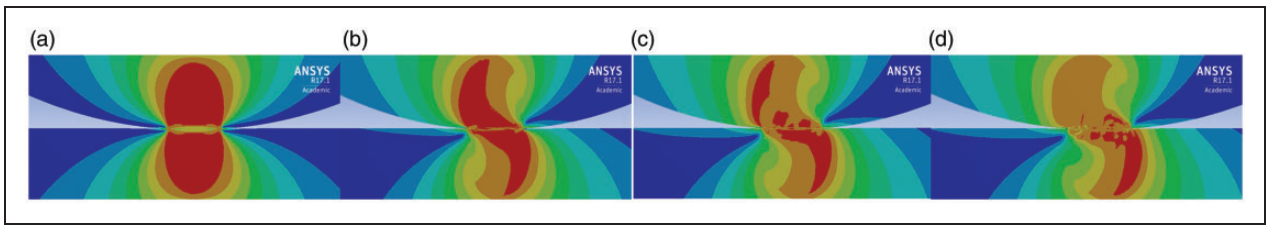

Figure 3. The distribution of von Mises stresses at $3^*\omega_{c1}$ interference with $\mu = 0.3$ for scheme 1 (steels): (a) sliding distance $0^*\omega_{c1}$; (b) sliding distance $1^*\omega_{c1}$; (c) sliding distance $1.5^*\omega_{c1}$; (d) sliding distance $5^*\omega_{c1}$.

617-on-Incoloy 800H contacts in Yang and Green.[15] Both of the models have performed a mesh convergence for the pure elastic contact. Three theoretical values (load per unit length, contact width, and maximum contact pressure) from the theoretical equations (equations (1) to (4)) agree well with those obtained from ANSYS with different inputs of interference. The maximum difference is below 2.2%.

In addition, since there is no closed-form solution for elastic-plastic contacts under the combined load of normal and tangential loads, the elements of the mesh are iteratively refined by a factor of two until there is less than 1% difference in the contact width between iterations. Additionally, the region in contact is always confined within the refined mesh.

Results and discussion

The evolution of the von Mises stresses

Figure 3 shows the evolution of von Mises stresses at $3^*\omega_{c1}$ interferences with $\mu = 0.3$, for sliding contacts between identical steels during $5^*\omega_{c1}$ sliding to the right. In Figure 3(a), the interference is just applied and no relative horizontal motion is introduced. The distributions of the von Mises stress are identical in the cylinder and the block. Then, the cylinder starts to move to the right. The large von Mises stresses begin to skew to the left in the cylinder and to the right in the block as shown in Figure 3(b). It is attributed to the introduction of the tangential force at corresponding directions. When the cylinder moves $1.5^*\omega_{c1}$ to the right and further, the distribution of the von Mises stresses starts to be different at the two bodies. The largest von Mises tends to locate at the leading edge of the contact and the bulk material of the block just under the leading edges. The explanation is that the pileup, which appears at the leading edge of the contact (to be discussed in a later section), increases the normal stress in the Y direction and the traction shear stress, ultimately causing an increase in the von Mises stresses at the leading edge in both the cylinder and the block. Additionally, once sliding commences the von Mises stresses become large at both the trailing edge in the cylinder and at the leading edge in the block. Compounding these two effects causes a different von Mises stress pattern to emerge. The high von Mises stresses at the contact edges create hot spots for wear and fatigue, while fatigue is more likely to occur in the bulk material under the leading edge.

The evolution of the von Mises stresses in the similar case for sliding between Inconel 617 and Incoloy 800H at 800 °C is shown in Figure 4. Since the yield strength of the block is about one-third of that of the cylinder, the largest von Mises stress in the block reaches S_{y2} right after the vertical interference, and is maintained at S_{y2} throughout the entire sliding.

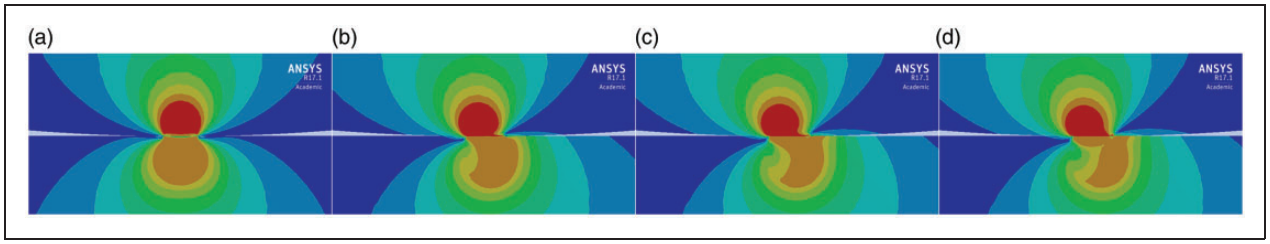

Figure 4. The distribution of von Mises stresses at $3^*\omega_{c2}$ interference with $\mu = 0.3$ for scheme 2 (alloys): (a) sliding distance $0^*\omega_{c2}$; (b) sliding distance $1^*\omega_{c2}$; (c) sliding distance $1.5^*\omega_{c2}$; (d) sliding distance $5^*\omega_{c2}$.

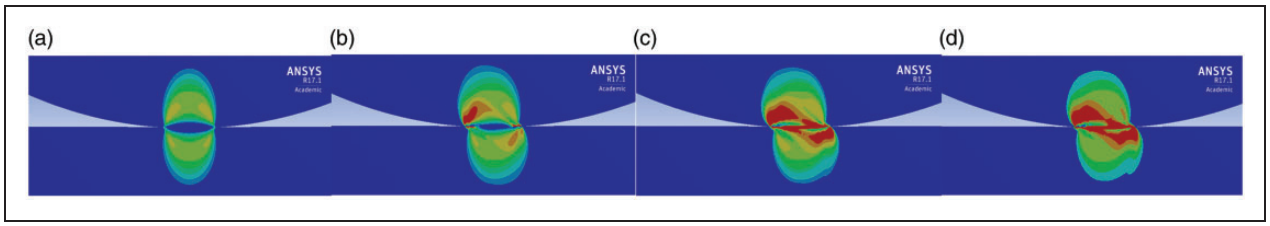

Figure 5. The distribution of plastic strains at $3^*\omega_{c1}$ interference with $\mu = 0.3$ for scheme 1 (steels): (a) sliding $0^*\omega_{c1}$, $\epsilon_{pmax} = 0.002$; (b) sliding $1^*\omega_{c1}$, $\epsilon_{pmax} = 0.01$; (c) sliding $2^*\omega_{c1}$, $\epsilon_{pmax} = 0.018$; (d) sliding $5^*\omega_{c1}$, $\epsilon_{pmax} = 0.61$.

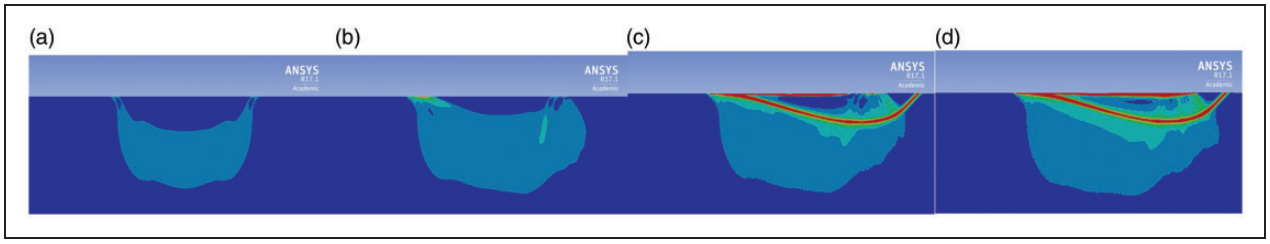

Figure 6. The distribution of plastic strains at $3^*\omega_{c2}$ interference with $\mu = 0.3$ for scheme 2 (alloys): (a) sliding $0^*\omega_{c2}$, $\epsilon_{pmax} = 0.002$; (b) sliding $1^*\omega_{c2}$, $\epsilon_{pmax} = 0.01$; (c) sliding $2^*\omega_{c2}$, $\epsilon_{pmax} = 0.018$; (d) sliding $5^*\omega_{c2}$, $\epsilon_{pmax} = 0.61$.

Although the largest von Mises stress in the cylinder keeps increasing during sliding, it never reaches the yield strength. The evolution of the von Mises stresses in the cylinder is similar to the case for contacts between steels as shown in Figure 3. One unique phenomenon in Figure 4 is that, at sliding distance of $1.5^*\omega_{c2}$ (Figure 4(c)), the large von Mises stresses (represented by deep orange) on the surface of the block spreads rapidly to the right compared with the distribution of the von Mises stresses at sliding distance of $1^*\omega_{c2}$ (Figure 4(b)).

The evolution of the equivalent plastic strains

Figure 5 shows the evolution of the equivalent plastic strains at $3^*\omega_{c1}$ interferences with $\mu = 0.3$, for sliding contacts between identical steels during $5^*\omega_{c1}$ sliding to the right. The maximum plastic strain keeps increasing during the sliding. Initially, the plastic strain is identical in the cylinder and the block, as shown in Figure 5(a). Then, there are large plastic strains appearing on the right edge of the contact in the block and the left edge of the contact in the cylinder, as shown in Figure 5(b). As the cylinder slides to the right further, the large plastic strain starts to appear along the whole contacting surface, and the distribution of the large plastic strain forms a "pocket" in the two bodies.

The evolution of the plastic strains in the case for sliding between Inconel 617 and Incoloy 800H at 800 °C is shown in Figure 6. Since the cylinder never yields as discussed in the previous section, there is no plastic strain in the cylinder, which is, hence, hidden in Figure 6. The distribution of the large plastic strain forms similar "pockets" in Figure 5(c) and (d). There are large plastic strains along the whole contacting surface, too.

Junction growth

During the sliding motion, the contacting surface deforms plastically as discussed in the previous section. As a result of that plastic deformation, the junction growth, i.e. the increase of the contact area, is observed. The contact area is defined as the surface of the cylinder where the pressure is not zero.

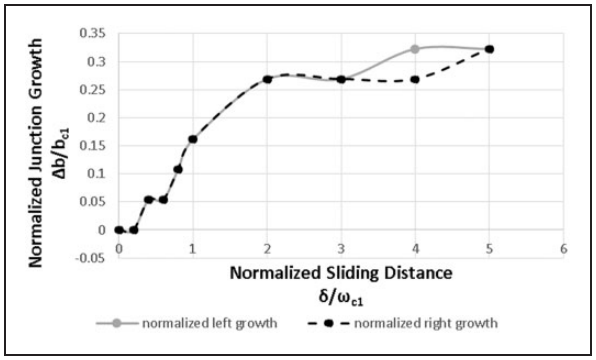

Figure 7. Junction growth on the two sides of the contacting area during $\delta = 5^*\omega_{c1}$ sliding at $\omega = 3^*\omega_{c1}$ interference with $\mu = 0.3$ for scheme 1 (steels).

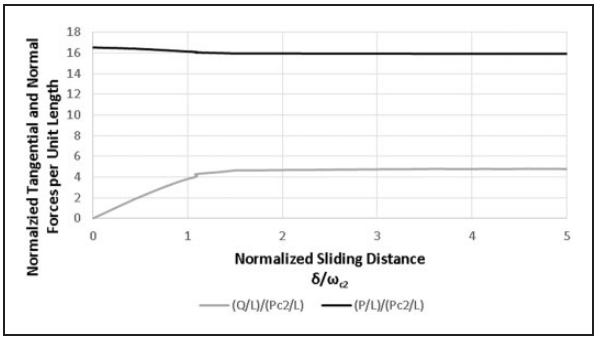

Figure 9. Evolution of the normalized tangential force $(Q/L)/(P_{c2}/L)$ and normalized normal force $(P/L)/(P_{c2}/L)$ during $\delta = 5^*\omega_{c2}$ sliding at $\omega = 3^*\omega_{c2}$ interference with $\mu = 0.3$ for scheme 2 (alloys).

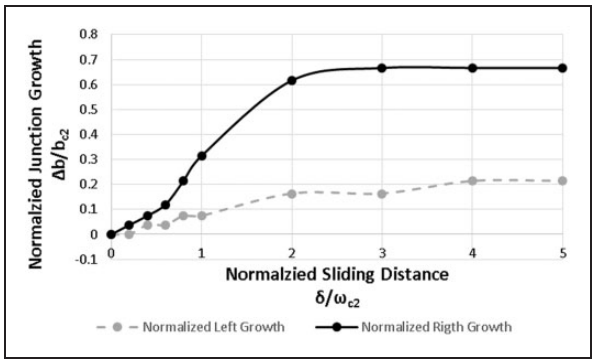

Figure 8. Junction growth on the two sides of the contacting area during $\delta = 5^*\omega_{c2}$ sliding at $\omega = 3^*\omega_{c2}$ interference with $\mu = 0.3$ for scheme 2 (alloys).

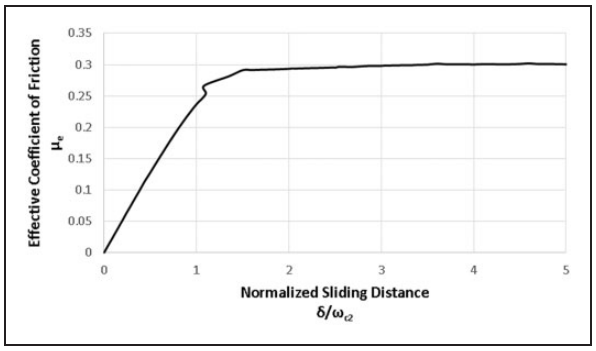

Figure 10. Evolution of the effective COF during $5^*\omega_{c2}$ sliding at $3^*\omega_{c2}$ interference with $\mu = 0.3$ for scheme 2 (alloys).

With respect to the original area in contact after the pure normal interference, the growing of the contact area takes place on both the positive and negative directions of the X-axis, which are implicitly represented as ''right'' and ''left'', respectively.

Figure 7 shows the junction growth at the two sides of the contacting area during $\delta = 5^*\omega_{c1}$ sliding at $\omega = 3^*\omega_{c1}$ interference with $\mu = 0.3$ for steels. The variable Δb represents the increase of the absolute value of the horizontal coordinate of the edges of the contact with respect to the values after the pure normal critical interference. The growth at the two edges contributes to the junction growth at almost the same magnitude, which is reasonable considering the identical materials of the two contacting bodies. According to the results, the junction growth does not seem to stabilize in Figure 7 after $5^*\omega_{c1}$ sliding.

Figure 8 shows the junction growth on the two sides of the contacting area during $\delta = 5^*\omega_{c2}$ sliding at $\omega = 3^*\omega_{c2}$ interference with $\mu = 0.3$ for alloys. The right side contributes to the growth more pronouncedly, and it is in the same direction of the tangential force experienced by the surface of the block. More generally, the more pronounced growth takes place in the same direction of the tangential force experienced by the weaker material (Incoloy 800H). Additionally, the junction growth stabilizes after $\delta = 5^*\omega_{c2}$ sliding as evident in Figure 8.

Evolution of tangential, normal forces, and effective COFs

Figures 9 and 10 show the evolution of the tangential force, the normal force, and the effective COF during $\delta = 5^*\omega_{c2}$ sliding at $\omega = 3^*\omega_{c2}$ interference with $\mu = 0.3$ for scheme 2. The effective COF, $\mu_e = (Q/L)/(P/L)$, is the actual ratio of the tangential force per unit length to the normal force per unit length. Although a constant COF is input in the interface of the contact, the effective COF is not always equal to the applied COF due to partial slip contact status at the beginning of the contact. Since it is a displacement-controlled motion, the normal force keeps decreasing because of the cylinder being flattened during the sliding. The three values stabilize between $1^*\omega_{c2}$ to $2^*\omega_{c2}$ sliding distance. It is corresponding to the position where the large von Mises stresses on the surface of the block spreads rapidly to the right, as shown in Figure 4. Based on the sliding status from ANSYS, this position is partial slip and partial stick, but its stick area starts to move along with the bulk material. Therefore, it is concluded that the forces

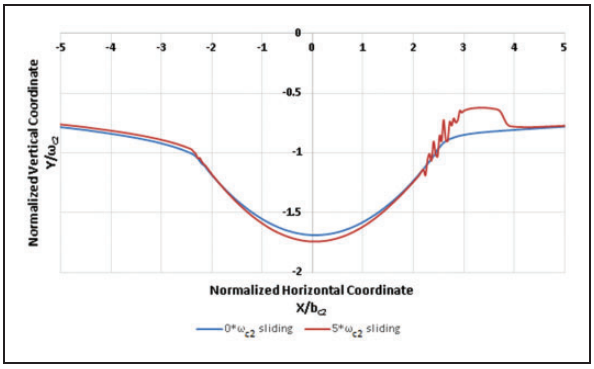

Figure 11. The evolution of scars on the surface of the block during $5^*\omega_{c2}$ sliding at $3^*\omega_{c2}$ interference with $\mu = 0.3$ for scheme 2 (alloys).

stabilize when the contacting area starts to move along with the sliding motion. Additionally, the effective COF converges to the value of the COF applied to the model, which means the frictional force is the dominant force in the tangential direction. Similar results have been found in the cases for steels.

Scars on the surface of the block

As the sliding motion proceeds, a scar is generated on the surface of the flat block. The scar can be visualized by the deformed curve of that surface. Figure 11 shows the deformed curves on the surface of the block at $\omega = 3^*\omega_{c2}$ interference during $\delta = 5^*\omega_{c2}$ sliding with $\mu = 0.3$ for scheme 2. When the $3^*\omega_{c2}$ interference is just applied, the normalized deformation at the center of the surface of the block is about $1.7^*\ \omega_{c2}$, which is larger than half of the applied interference, $3^*\omega_{c2}$. That is caused by the plastic deformation on the block, while the cylinder deforms entirely elastically. After the cylinder slides $\delta = 5^*\omega_{c2}$ to the right, there is pileup showing up at the leading edge of the contact. The pileup contributes to the large von Mises stresses and large plastic strains showing up at the leading edge of the contact.

Conclusion

This work presents a 2D plane strain finite element sliding contact model of a half-cylinder in contact with a block. The materials of the two bodies are identical steels or special alloys (Inconel 617 and Incoloy 800H at 800 °C). The two schemes represent the two cases, one for contacts between identical materials and the other one for a hard indenter over a weaker bulk material. The sliding model is displacement-controlled, where it is loaded with an interference first, and then a one-sided horizontal displacement is applied to the top of the half cylinder. The contact is in the regime of elastoplastic contacts. Several conclusions are drawn:

1. The large von Mises stresses stay on the leading edge of the contact and the bulk material under the leading edge for the two schemes. Should wear and fatigue occur by the sliding contact, they are most likely to appear at the above location.
2. The large plastic strains are shown on the surface of the sliding contact. A "pocket" formed by the large plastic strains shows up as the sliding proceeds over a sufficient distance. The "pocket" is more pronounced in scheme 2.
3. The junction growth is obtained during the sliding motion. For scheme 1, growths on the two sides are in the same magnitude, while for scheme 2, the growth on the right side is more pronounced. It can be concluded that the more pronounced growth on the two edges is in the same direction of the tangential force experienced by the surface of the deformed body. This conclusion agrees with the results of Brizmer et al.[8] whose model is the contact between a deformable sphere and a rigid flat under full stick condition.
4. The normal force, tangential force, and the effective COF stabilize at the sliding distance between $1^*\omega_c$ to $2^*\omega_c$ when the contact area starts to move along the bulk material. The effective COF converges to the COF applied to the model, which means the friction force is the dominant force in the tangential direction.
5. There are pileups appearing on the surface of the block, which is located at the leading edge of the contact.

Declaration of Conflicting Interests

The author(s) declared no potential conflicts of interest with respect to the research, authorship, and/or publication of this article.

Funding

The author(s) disclosed receipt of the following financial support for the research, authorship, and/or publication of this article: This research was supported by the Department of Energy under Project 2506U87, Award RH452.

References

1. Johnson KL. *Contact mechanics*. Cambridge: Cambridge University Press, 1987.
2. Chang L and Zhang H. A mathematical model for frictional elastic-plastic sphere-on-flat contacts at sliding incipient. *J Appl Mech* 2007; 74: 100–106.
3. Scheibert J, Prevost A, Debrégeas G, et al. Stress field at a sliding frictional contact: experiments and calculations. *J Mech Phys Solids* 2009; 57: 1921–1933.
4. Courtney-Pratt J and Eisner E. The effect of a tangential force on the contact of metallic bodies. *Proc Roy Soc Lond A* 1957; 238: 529–550.
5. Tabor D. Junction growth in metallic friction: the role of combined stresses and surface contamination. *Proc Roy Soc Lond A* 1959; 251: 378–393.
6. Parker R and Hatch D. The static coefficient of friction and the area of contact. *Proc Phys Soc B* 1950; 63: 185.

7. Bellemare S, Dao M and Suresh S. Effects of mechanical properties and surface friction on elasto-plastic sliding contact. *Mech Mater* 2008; 40: 206–219.
8. Brizmer V, Kligerman Y and Etsion I. A model for junction growth of a spherical contact under full stick condition. *ASME Trans J Tribol* 2007; 129: 783–790.
9. Diao D. Finite element analysis on local yield map and critical maximum contact pressure for yielding in hard coating with an interlayer under sliding contact. *Tribol Int* 1999; 32: 25–32.
10. Ronen S, Goltsberg R and Etsion I. A comparison of stick and slip contact conditions for a coated sphere compressed by a rigid flat. *Friction* 2017; 5: 326–338.
11. Holmberg K, Laukkanen A, Ronkainen H, et al. Tribological contact analysis of a rigid ball sliding on a hard coated surface: part I: modelling stresses and strains. *Surf Coat Technol* 2006; 200: 3793–3809.
12. Vijaywargiya R and Green I. A finite element study of the deformations, forces, stress formations, and energy losses in sliding cylindrical contacts. *Int J Non-Linear Mech* 2007; 42: 914–927.
13. Tian H and Saka N. Finite element analysis of an elastic-plastic two-layer half-space: sliding contact. *Wear* 1991; 148: 261–285.
14. Yang H and Green I. An elasto-plastic finite element study of displacement-controlled fretting in a plane-strain cylindrical contact. *ASME Trans J Tribol* 2018; 140: 041401.
15. Yang H and Green I. A fretting finite element investigation of a plane-strain cylindrical contact of Inconel 617/ Incoloy 800H at room and high temperature. *Proc IMechE, Part J: J Engineering Tribology* 2018; 233: 1–17.
16. Special-Metals. Product handbook of high performance nickel alloys. Product Handbook of a PCC Company, 2008.
17. Green I. Poisson's ratio effects and critical valus in spherical and cylindrical Hertzian contacts. *Appl Mech Eng* 2005; 10: 451.

Appendix

Notation

b	half-contact width
b_c	critical half-contact width
C	Poisson's ratio parameter
E_1	elastic modulus of the cylinder
E_2	elastic modulus of the block
E'	equivalent elastic modulus
p_0	maximum contact pressure
p_{0c}	critical maximum contact pressure
P/L	normal force per unit length
P_c/L	critical normal force per unit length
Q	tangential force
R	radius of half-cylinder
S_y	yield strength
δ	horizontal displacement
μ	coefficient of friction
μ_e	effective coefficient of friction
ν_1	Poisson's ratio of the cylinder
ν_2	Poisson's ratio of the block
ω	interference
ω_c	critical interference
ω^*	normalized interference, $\omega/\ \omega_c$
ε_{p}	equivalent plastic strain
$\varepsilon_{\mathrm{pmax}}$	maximum equivalent plastic strain